









A Renewable Energy Source Fed Neuro-Fuzzy Controlled Multilevel UPQC for Power Quality Improvement

Koganti Srilakshmi * , M. Mallikarjuna Reddy ** , Krishnaveni Bukkapatanam *** , B. Madhu Kiran**** , Gondi Konda Reddy ***** , Gangapuram Srikath ***** , G. Deepika ***** , Surender Reddy Salkuti***** 

* Department of Electrical and Electronics Engineering, Sreenidhi Institute of Science and Technology, Hyderabad, Telangana, India.

** Department of Electrical and Electronics Engineering, SIR C R Reddy College of Engineering, Eluru, A.P, India

*** Department of Electrical and Communication Engineering, Sreenidhi Institute of Science and Technology, Hyderabad, Telangana, India.

**** Department of Electrical & Electronics Engineering, Seshadri Rao Gudlavalluru Engineering college, AP, India.

***** Department of Mechanical Engineering, Sreenidhi Institute of Science and Technology, Hyderabad, Telangana, India

***** Department of Electrical & Electronics Engineering, Geethanjali college of Engineering and Technology, Hyderabad, Telangana, India.

***** Department of Electronics and Communication Engineering, St. Peters Engineering College, Telangana, India

***** Department of Railroad and Electrical Engineering, Woosong University Daejeon, Republic of Korea

(kogantisrilakshmi29@gmail.com, mallikarjuna.madire@gmail.com, sriveniz@gmail.com, mkbaba9@gmail.com, kondareddy@reenidhi.edu.in, gsrikanth.eee@gcet.edu.in, gdeepika@stpetershyd.com, surender@wsu.ac.kr)

†

Corresponding Author: Koganti Srilakshmi, Department of Electrical and Electronics Engineering, Sreenidhi Institute of Science and Technology, Hyderabad, Telangana, India, Tel: +91-8885851666.

kogantisrilakshmi29@gmail.com.

Received: 08.08.2023 Accepted: 20.09.2023

Abstract: Recent days, integration of renewable sources plays a key role in distribution network to supply the demand effectively. The usage of power electronics gadgets and non linear loads leads to the generation of harmonics. This work develops the H-Bridge cascade five-level unified Power quality conditioner coupled with photovoltaic and battery storage systems to handle the power quality related problems. To eliminate the requirement of the complex transformations like abc, dq0, $\alpha\beta$, the artificial neural network-based control scheme with LMBP training method is adopted for the 5L-UPQC to produce the necessary reference signals for the shunt and series voltage source converters. In addition, an adaptive neuro-fuzzy controller is suggested for DC link error current minimization, which utilizes the properties of both the fuzzy as well as ANN. The main aim of the developed scheme is to maintain constant DLCV in load changes, diminish of THD in the source current and load voltage, and maximum elimination of supply voltage fluctuations like sag/swell and disturbances. The suggested method was demonstrated in four cases with several permutations of loads. However, to reveal the performance of the developed method, the comparison is carried out with the PIC and SMC and along with two level and three level UPQC configurations in addition to the controllers available in literature. The suggested technique diminishes the THD to 2.26%, 2.12%, 3.73%, and 1.59% which are lesser than the controllers that are available in the survey of literature. The design has been performed on MATLAB/simulink software.

Keywords- Total Harmonic Distortion, Shunt Active Power Filter, and Series Active Power Filter, Swell, Unified Power Quality Conditioner, Sag.

Nomenclature:

Five-level-UPQC	5L-UPQC	IL	Input layer of ANN
PV	Photovoltaic	HL	Hidden layer of ANN
BSS	Battery storage system	E	Error
PQ	Power Quality	L_{se}	SEAF Inductance
ANN	Artificial neural network	V_{S_abc}	Source voltage for abc phases
UPQC	Unified Power quality conditioner	V_m	Peak voltage of the system
LMBP	Levenberg- marquardt back propagation	R_S, L_S	Grid Resistance and Inductance
p-q	Instantaneous reactive power	m	Modulation index
DLCV	Direct current link capacitor voltage	V_{l_abc}	Load voltage for phases a, b, c
SRF	Synchronous reference frame	C_{dc}	DC link capacitance
THD	Total harmonic distortion	V_{se_abc}	Voltage injected by series filter in abc
PF	Power factor	$V^{ref}_{se_abc}$	Reference compensated voltage in abc phase
GA	Genetic algorithm	i_{S_abc}	Source current for abc phases
PSO	Particle swarm optimization	i_{l_abc}	Load current for abc phases
PIC	Proportional integral controller	R_{sh}	SHAPF Resistance
SHAPF	Shunt Active Power Filter	f_{sh}, f_{se}	Switching frequency
GWO	Grey wolf optimization	$V_{cr,pp}$	Peak-to-peak voltage ripple
PWM	Pulse width modulation	V_{dc}	DC link voltage
BBC	Buck-boost converter	a_f	Overloading factor
SMC	Sliding mode control	V^{ref}_{dc}	Reference DLCV
FLC	Fuzzy logic controller	i_{sh_abc}	Shunt filter compensated current in abc
VSC	Voltage source converter	Δi_{dc}	DC link output error
MSE	Mean square error	$i^{ref}_{sh_abc}$	Shunt filter reference compensated current in abc phases
BBO	Biogeography based optimization	i^{ref}_{dc}	Reference DC current
SEAF	Series Active Power Filter	R_{se}	SEAF Resistance
BC	Boost converter	$V_{dc, err}$	DLCV error
ACO	Ant colony algorithm	$i^{ref}_{BS, er}$ *	Reference battery error current
SCC	Short circuit current	i_{ph}	Photocurrent source
FOPID	Fractional order proportional integral derivate	i_{PV}	PV cell output current
MSF	Membership function	L_{sh}	SHAPF Inductance
ANFIS	Artificial neuro-fuzzy interface system		
FF-ANN	Firefly based ANN		
PPFFA	Predator-prey firefly algorithm		
SPG	Solar power generation		
V _{LL}	Line to Line rms voltage		
CE	Change in error		
OL	Output Layer of ANN		

$R_{s,PV}$ and $R_{sh,PV}$	Resistances of PV cells in series and parallel
i_{BS}^{ref}	Reference current of battery
i_d	Forward diode carrying current
$i_{sh,PV}$	Parallel current of PV cell
$i_{BS,err}$	Battery error current
Δi_{lmax}	Peak ripple current
T_C	Cell's temperature
η	Diode ideal factor
N_s	Number of PV cells connected in series
Q	Electron charge
k	Boltzmann's constant
G, G_n	Solar irradiance (W/m^2) and at STC
P_{PV}	Solar PV power output
ΔT_C	Change in PV cell's temperature
$i_{PV,m}, V_{PV,m}$	Module current and voltage
P_{dc}	DC link power
i_b	Battery current
E_0	Batteries' constant voltage
$i_{s,PV}$	Reverse saturation current
P_{BS}	Batter's output power
R	Internal batteries' resistance
ΔV_{PV}	Change in PV voltage
SOC_{OB}	State of charge of battery
$E_{f1,2}(i_t, i_h, i_b)$	No load battery voltage
Q	Battery capacity
Δi_{PV}	Change in PV current

In recent years, integrating renewable energy systems like solar and wind into the distribution network has been encouraged to reduce the stress on converters and ratings. The output of a traditional square-wave inverter is a square wave with a significant amount of harmonics. This necessitates the use of large-area filters to tailor the output and create sinusoidal shape. When employing traditional square-wave inverters, the cost and size of the filter rise, which becomes a significant disadvantage. The admirable properties of multi-level inverters that produce leveled output. Compared to traditional square-wave inverters, leveled output requires smaller filters.

The solar-integrated UPQC was developed to address PQ issues efficiently. In order to obtain the most power and maintain DLCV balance, a unique fuzzy-based PIC was created for the Maximum power tracking technique [1]. In addition, an innovative hybrid enhanced method for the SHAPF connected with ANN technology was introduced to minimize current waveform flaws and boost PQ in the distribution network [2]. The best tuning of a fractional order proportional integral controller for reactive power and harmonic compensation under balanced and unbalanced loading conditions was then used to construct the PSO and GWO-based optimal SHAPF, which was then tested experimentally [3]. However, using hysteresis and PWM approaches, the effectiveness of wind systems associated with UPQC was investigated under various loads and problematic conditions [4]. Additionally, using the technique of impedance matching, the power flow analysis of the UPQC was examined on a three-phase distribution network under different operating conditions [5].

Additionally, the power flow analysis of the UPQC was investigated on a 3-phase distribution grid under various operating situations using the method of impedance matching [6]. Besides, the fuzzy-based hybrid technique was adopted to achieve maximum out of PV. However, to reduce the complexity the ANN was considered for UPQC reference signal generation to sole PQ issues [7]. To reduce the current THD, the intelligent fuzzy-tuned PIC was created for the hybrid shunt active and passive filters. By utilizing Clarke's transformation, the performance study was done for various loads [8]. The Solar PV-powered UPQC was also introduced to lower grid current THD during voltage variations like sag and swell by utilizing ANN. Additionally, under various load conditions, the proposed method was contrasted with SRF and p-q methods [9]. The hybrid fuzzy PIC was suggested for wind and battery integrated UPQC to address PQ issues effectively [10]. However, to regulate DLCV and to handle power feed forward ANN has been suggested for PV/wind associated UPQC [11].

To lower THD in the grid current waveform, the H bridge inverter-based single phase SHAPF with a modified Predictive Current Control approach was introduced [12]. Future, the microgrid-connected multilevel DSTATCOM was developed to eliminate voltage and current distortions effectively [13]. Future, a comprehensive study was done on various phase synchronisation techniques used to control the working of SHAPF [14]. The novel technique was introduced for the

1. Introduction

UPQC to improve power quality to regulate energy transfer between sources and loads [15].

For the AC-DC micro-grid system, intelligent hybrid controllers such as fuzzy-PIC and fuzzy PID controllers were developed to increase PQ and stabilize voltage in the presence of D-STATCOM. [16]. However, the GWO was suggested to optimize the gain parameters of PIC based UPQC to reduce THD for both linear and non-linear loads [17]. Hysteresis current control was used for pulse generation, stabilizing the DLCV for SHAPF to effectively deal with PQ issues. Additionally, linear and non-linear loads were considered to study performance [18]. The BBO was selected to obtain optimal gain values of PIC and for fast action in fault identification with higher accuracy with a motive of stabilizing DLCV fluctuations [19].

The hybrid fuzzy ANN control technique has been adopted for UPQC to minimize the current THD and voltage fluctuations and improve network usage [20]. The Improved bat and Moth Flame metaheuristic optimization methods were hybridized to solve the PQ issues by optimal selecting the gain values of PIC [21]. The FLC was developed for SEAF of the distribution network to minimize the current and voltage-related PQ problems [22].

The predator-prey firefly algorithm was selected for the optimal selection of gain parameters of PIC adapted to the SHAPF to reduce the THD and to enhance the PF [23]. A Soccer match optimization for the optimal selection of weights for the ANN controller was suggested for PV/battery-associated UPQC to solve PQ issues [24]. The ACO was chosen for selecting the K_p , K_i values of PIC for the SHAPF to reduce THD under several loading conditions [25]. An adaptive novel hysteresis band with FLC was suggested to the PV-powered 9-level VSC of UPQC to receive fluctuations free signals [26]. Next, the Soccer match optimization was proposed for the appropriate selection of PIC gain parameters for UPQC to successfully handle both voltage fluctuations and current distortions [27].

For UPQC, the hybrid control strategy combining FLC and ANN features was suggested as a way to lessen the flaws in the grid's voltage and current waveforms while still maintaining DLCV for dynamic loads [28]. The ANN based method was suggested for five-level UPQC to control the PQ problems [29]. The firefly based optimization was used to train ANNC was developed for the shunt VSC for the PV/battery UPQC to reduce the MSE and minimize THD [30]. The self tuning filter based method was developed for UPQC integrated with renewable sources to address PQ issues [31]. The LMBP-trained ANN controller was adopted for UPQC to mitigate current and voltage-related PQ problems efficiently [32].

It was investigated [33] the advantages and difficulties of integrating renewable energy sources into the system and their control strategies. A few recommendations were also made to transform the conventional grid into a smart grid, and the implications of smart grid technologies on the national grid were underlined [34]. For changes in solar irradiation, the

comparison of P & O and PSO algorithms to provide MPP for the PV system was investigated [35]. Integration of renewable sources to micro grid for MPPT was studied with power management [36]. High voltage isolated ACDC converters were developed based on the modular technology [37]. Fuzzy logic controller was suggested for PV-MPPT to improve the overall performance by maximum power point tracking [38].

The literature listed in Table 1 makes it abundantly evident that the majority of the works mostly concentrated on different controllers using the pre-existing traditional control methods for UPQC that included complicated parks and Clarke's transformations. In addition to an ANFIS controller for DC link balancing, this publication develops an ANN-based reference signal generation for PV/battery-coupled DC link UPQC.

The novelty of this manuscript is highlighted in the steps below:

- Developing the H-bridge cascade five level VSC for UPQC for effectively reducing imperfections in waveforms effectively.
- Introducing the LMBP trained ANNC for generating effective reference signals in order to eliminate the necessity of complex abc-dq0- $\alpha\beta$ 0 conversions i.e SRF and p-q theories.
- Proposing the hybrid ANFIS controller to maintain constant DLCV.
- Incorporating the solar PV and battery systems to the DC link of 5L-UPQC to reduce the stress and burden on VSC, supports to meet the load demand, and maintain constant DLCV during load variations.
- The objective of the proposed system is to diminish the source current THD, and eliminating the grid voltage side troubles like (disturbance, swell, sag etc.)
- Additionally, the suggested ANFIS scheme for 5L-UPQC with PV and BES (5L-UPQC) is examined on 4-test cases for several types of loads and irradiation to show its superior performance.
- The concept was tested by comparing it standard PIC and SMC controllers with three and two level converters and with SRF and p-q theory.

This paper is structured as follows, section 2 gives the modeling of 5L-UPQC, Section 3 explains the proposed control scheme, Section 4 demonstrates the results and discussion, and Section 5 concludes the manuscript.

2. Modelling of Developed 5L-UPQC

Figure 1 shows the proposed 5L-UPQC configuration, which connects the PV and batteries to the DC link of the UPQC. Combining series and shunt VSCs creates UPQC. By supplying the appropriate compensation voltage via the injecting transformer and the inductor, the SHAPF seeks to resolve grid-side voltage-related issues. The SHAPF is similarly connected to the grid via the interface inductance. By injecting a sufficient compensating current, the SHAPF seeks to decrease the current waveform harmonics and maintain DLCV constant with a minimal settling time.

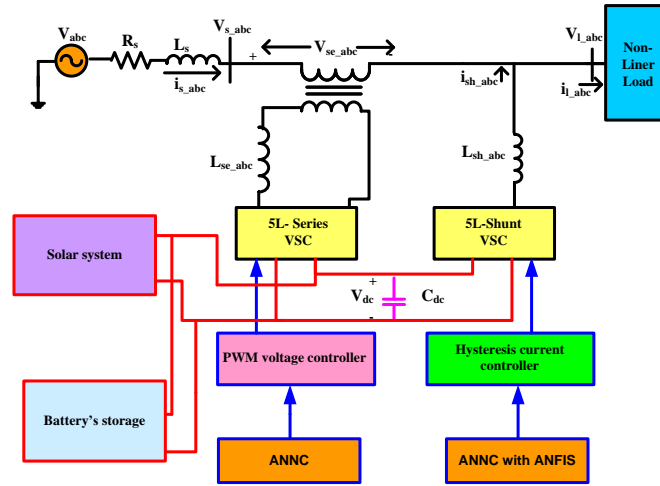


Fig. 1. Proposed 5L-UPQC configuration

Table 1: A literature survey (current start of art)

Ref/ year [No]/Year	Control		PQ Issues				Loads	
	Reference signal generation	Controller	THD	DLCV balancing	Supply Voltage sag, swell	Supply Voltage disturbance	Non-linear sensitive load	Unbalanced load
[3] / 2020	p-q theory	FOPID	✓				✓	✓
[4]/ 2022	SRF	PIC	✓					
[7]/ 2023	ANN	ANN	✓	✓	✓	✓	✓	✓
[8]/ 2022	SRF	FUZZY-PI	✓	✓			✓	
[11]/ 2021	ANN	ANN	✓		✓		✓	✓
[19]/ 2021	SRF	PI-BBO	✓		✓		✓	✓
[21]/2021	SRF	ANFIS	✓				✓	✓
[22]/2018	p-q	FUZZY	✓		✓		✓	
[23]/ 2019	SRF	PPFFA	✓				✓	✓
[25]/2019	SRF	PI-ACO	✓				✓	✓
[29]/ 2017	ANN	ANN	✓	✓	✓		✓	✓
[30]/2023	SRF	FF-ANN	✓	✓	✓	✓	✓	✓
Proposed 5L-UPQC	ANNC	ANFIS	✓	✓	✓	✓	✓	✓

One of the best structures is the multi-level inverter cascaded H-Bridge topology, which requires no clamping tools or components. Although the Cascaded H-Bridge topology's layout is straightforward, more DC sources are needed to power each single H-Bridge cell. Two H-Bridge cells are cascaded into a five-level H-Bridge structure, and every single H-Bridge cell is powered by a DC source. Figure 2 displays a multi-level inverter five-level cascaded H-Bridge arrangement. Figure 2 also displays the cascaded H-Bridge's 5L voltage output in phase. The five-level output is produced by sequentially triggering power switches as the whole DC link voltage is divided across two H-Bridge cells. Figure 2

shows the power switches used for 5-level Cascaded H-Bridge and it's switching order in given in Table 2.

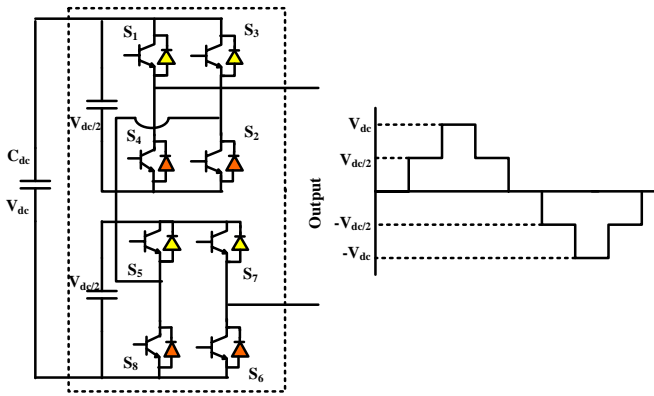


Figure 2: Proposed 5L-cascade H bridge UPQC with output

2.1 Selection of C_{dc} and V_{dc}

From [29], under faulty conditions, assume the shunt and series VSC’s power handling capacities are 0.5XkVA and 2XkVA, respectively. The kVA rating of VSC and V_{dc} is inversely proportional. By the change of 25% of V_{dc} , the equivalent change in the energy across C_{dc} is calculated by Eq. (1)

$$\Delta E_{dc} = 1 / 2C_{dc} [(1.125V_{dc})^2 - (0.875V_{dc})^2] \quad (1)$$

Table 2: ON/OFF of switches considered for 5L- cascaded Hbridge UPQC

Output Voltage	S1	S2	S3	S4	S5	S6	S7	S8
V_{dc}	1	1	0	0	1	1	0	0
$V_{dc}/2$	1	1	0	0	1	0	1	0
0	1	0	1	0	1	0	1	0
$-V_{dc}/2$	0	0	1	1	1	0	1	0
$-V_{dc}$	0	0	1	1	0	0	1	1

*Note: 0=Off, 1=On

Assume that for the suppose the load changes from 2XkVA to 0.5XkVA in ‘n’ cycles in ‘T’ sec, then the corresponding change in the system’s energy is given by

$$\Delta E_s = (2X - X / 2)n.T \quad (2)$$

By, equating Eq. (1) and (2), the C_{dc} is given by Eq. (3)

$$C_{dc} = \frac{2(2X - X / 2)n.T}{(1.125V_{dc})^2 - (0.875V_{dc})^2} \quad (3)$$

Let, V_{dc} is m times to V_m . Where, ‘m’ modulation index varies between 1.2 and 2. However, %THD depends on L_{sh} and V_{dc} so the value of m is selected as 1.6 [29] for minimum THD. Therefore, V_{dc} is given by Eq. (4)

$$V_{dc} = 1.6 * V_m \quad (4)$$

The V_{dc} for n level converter is evaluated by using [29] Eq. (5)

$$V^{ref}_{dc} = V_{dc} / (n - 1) \quad (5)$$

2.2 Selection of coupling inductors for Shunt and series VSC

The coupling inductors adopted to connect the series and shunt VSC’s to the source and the load are limited by di/dt and magnitude of currents. The Δi_{lmax} occurs at $m=0.5$, given in Eq. (6) is controlled by PWM [29].

$$\Delta i_{lmax} = V_{dc} / 6f_{sw}L_{se} \quad (6)$$

Assuming the ripple current is about 10% of the maximum peak-to-peak current given by Eq. (7)

$$\Delta i_{lmax} = 0.1 * i_{max} \quad (7)$$

Therefore, the maximum current handling by a series capacitor in terms of power and phase voltage is given by Eq. (8). By using Eq. (6) and (8) L_{se} can be calculated.

$$i_{max} = \frac{\sqrt{2} * P_r}{3 * V_{ph}} \quad (8)$$

By heuristically testing [29] it has been identified that for $m=1.6$, $V^{ref}_{dc}=700$, and $L_{sh}=15$ mH the % THD is lower. The value of L_{sh} is given by Eq. (9)

$$i_{max} = \frac{V_{dc}}{4.h.f_{swmax}} \quad (9)$$

Where, h is the hysteresis band 5-10%.

2.3 Modelling of external support of 5L-UPQC

The solar/battery-fed DC link is proposed for the diode clamped 5L-UPQC. It consists of a hybrid solar and battery energy system to regulate the DLCV during the variation in loads. External support can reduce the converter ratings and stress by lowering the utility's demands. The equation for DC link power demand (P_{dc}) of the suggested technique is given in equation (10).

$$P_{PV} + P_{BSS} - P_{dc} = 0 \quad (10)$$

2.3.1 Solar power generation system (SPG)

The PV model used in this work was selected from the Simulink library. To create the necessary quantity of voltage and current, the PV models are connected in series to form a string. Some of these strings are then connected in parallel. A single-diode equivalent circuit is used to design each PV cell in the module, as seen in Fig. 3.

It comprises of a i_{ph} source carrying current through a forward diode and parallel and series cell resistances. Sunlight is recognized by the PV cell, which then transforms it into current. PV cell output current is obtained using KCL by Eq. (11)

$$i_{PV} = i_{ph} - i_d - i_{sh} \quad (11)$$

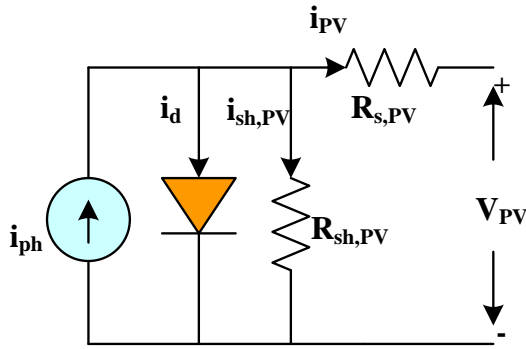


Figure 3: PV cell model

The current of a cell is derived by Eq. (12) by replacing the equations for i_d and i_{sh} .

$$i_{PV,c} = i_{ph} - i_{s,PV} \left[\exp\left(\frac{Q(V_{PV} + (i_{PV,c}R_{s,PV}))}{\eta k T_C}\right) - 1 \right] - \frac{V_{PV,c} + (i_{PV,c}R_{s,PV})}{(R_{sh,PV})} \quad (12)$$

However, PV cells are connected in series to form a module whose output is given by Eq. (13)

$$i_{PV,m} = i_{ph} - i_{s,PV} \left[\exp\left(\frac{Q(V_{PV} + (i_{PV,m}R_{s,PV}))}{\eta k T_C}\right) - 1 \right] - \frac{V_{PV,m} + (i_{PV,m}R_{s,PV})}{(R_{sh,PV})} \quad (13)$$

By using Eq. (14), the PV modules are attached in parallel and series to form an array.

$$i_{PV,n} = i_{ph}N_p - i_{s,PV}N_p \left[\exp\left(\frac{Q(V_{PV} + N_s/N_p(i_{PV,n}R_{s,PV}))}{N_s\eta k T_C}\right) - 1 \right] - \frac{V_{PV,n} + N_s/N_p(i_{PV,n}R_{s,PV})}{N_s/N_p(R_{sh,PV})} \quad (14)$$

Where,

$$i_{ph} = (i_{ph,n} + K_1\Delta T_C) \frac{G}{G_n} \quad (15)$$

Eq. (16) describes the solar output. Figure 4 illustrates the PV cell properties for a fixed temperature and changing irradiance.

$$P_{PV} = V_{PV} \times i_{PV} \quad (16)$$

2.3.2 Battery storage system (BSS)

The BSS aids in supporting the DLCV's stabilization. Cells are stacked in parallel or series in a battery to provide the necessary voltage and current. Since Li-ion batteries have benefits like slower discharge and inexpensive maintenance costs, this work chooses them from the Simulink library. The Li-ion battery's charging and discharging model is shown in Eq. (17).

$$V_b = E_{f1,2}(i_t, i_h, i_b) - iR \quad (17)$$

Following are the words used to define the Li-ion charging and discharging model with regard to of batteries E0 and Q

$$E_{f1}(i_t, i_h, i_b) = E_0 - K\left(\frac{Q}{0.1Q + i_t}\right)i_h - K\left(\frac{Q}{Q - \int i_t dt}\right)i_t + A \exp(-B \int i_t dt)$$

$$E_{f2}(i_t, i_h, i_b) = E_0 - K\left(\frac{Q}{Q + i_t}\right)i_h - K\left(\frac{Q}{Q - \int i_t dt}\right)i_t + A \exp(-B \int i_t dt) \quad (18)$$

The state of charge of battery (SOCOB) is expressed in Eq (19).

$$SOCOB = 50(1 + \int i_{BSS} dt Q) \quad (19)$$

The SPG will choose whether to charge or discharge the battery while adhering to the restrictions stated by Eq. (20). Fig. 5 depicts the battery's drain. Table 3 lists the ratings chosen for solar and battery systems. Table 4 displays the power division at DC's link capacitor. Fig. 6 shows the control mechanism for the solar and battery system fed to the DC link.

$$SOCOB_{min} \leq SOCOB \leq SOCOB_{max} \quad (20)$$

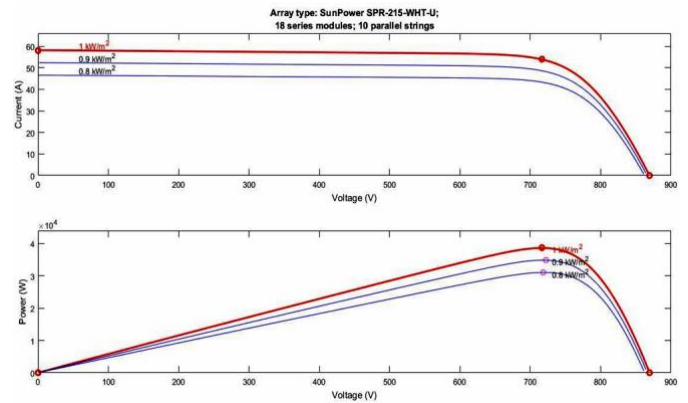


Figure 4: PV cell characteristics at various irradiation and constant temperature 25⁰c

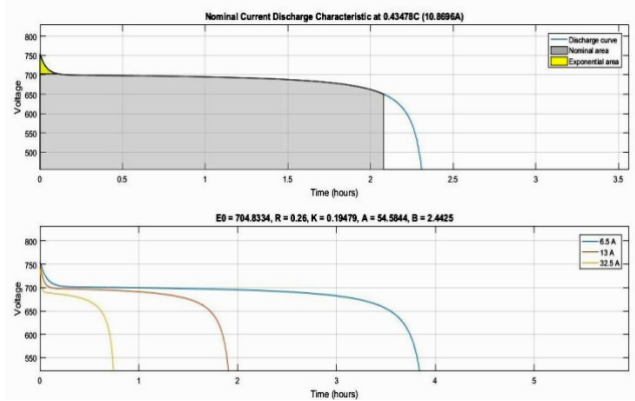


Figure 5: Li-ion battery characteristics for discharge

Table 3: Solar and BSS Ratings

Equipment	Factor	Value chosen
PV single panel (Sun power)	Rated Power	214.92W
	Open circuit voltage	39.8V
	Short circuit current	5.8A

SPR-215-WHT-U)	Under max power the voltage & current	39.8V /5.4A
	Number of PV cells assembled in parallel, series	11, 18
	Rated Capacity of battery	25Ah
Li-ion battery	Normal Voltage	650V
	Fully charge voltage	756.59V
	Cut off voltage	487 V

3. Proposed Control Scheme

Generally, chances take place at the distribution side during dynamic load variation. For a brief period, the system must be restored to its initial value in order to function normally. Here, using the recommended ANNC, the PWM approach generates gate pulses for the series VSC and PWM hysteresis current control for the shunt VSC.

3.1 Shunt VSC

The major objective of SHAPF is to manage DLCV under faults and dynamic loading circumstances and to suppress current signal distortions by injecting compensating current. The OL, IL, and HL components of ANN make up its structure. Where the IL gathers data supplied as input and sends it to the HL. When linked between the IL and HL, it is afterwards multiplied by the appropriate weights on the connected links. Here, calculations are performed with a chosen bias on HL, and the outcomes are gathered in OL.

In this case, LMBP-based ANN is chosen. To get the desired output, the weights of the link are adjusted during training by analysing the mistake. For ANN training where the performance function is MSE, the LMBP training method is used. The LMBP algorithm updates the weights using the obtained derivatives, which has the advantages of rapid convergence and effective learning.

Table 4: Power management at DC Link capacitor

Modes of operation	Action taken
Mode-1 : When No SPG	BES only will provide power to P_{DC} .
Mode-2 : When $SPG = P_{DC}$	Solar PV will supply power P_{DC} . The difference sum of the power will be provided by Battery till it reaches $SOCB_{min}$.
Mode-3 : When $SPG < P_{DC}$	Excessive solar power is utilized to charge the Battery system till it reaches $SOCB_{max}$.
Mode-4 : When $SPG > P_{DC}$	

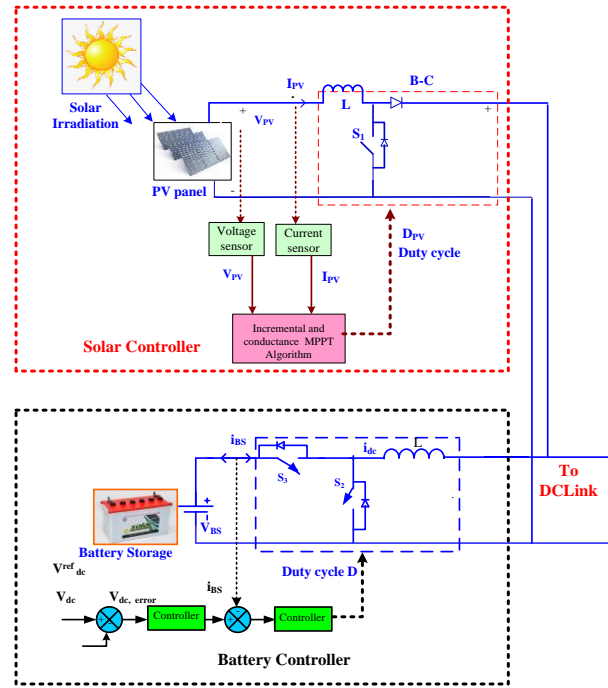


Figure 6: Controller of external supplies

3.1.1 ANFIS

The ANFIS is suggested to maintain constant DLCV. The suggested ANFIS is an intelligent hybrid controller with a combination of ANN and Fuzzy logic features. However, for maintaining DLCV constant, the chosen reference DLCV is compared to the obtained DLCV; its output E, CE is considered as input. The inputs fed to the ANNC are initially trained according to the triangular MSF to produce the best as shown in Figure 7. ANFIS mainly consists of five layers, the 1st layer (Fuzzification) the outputs of this layer are fuzzy MSF given by Eq. 21 shown in Fig. 7

$$\mu_{A_i}(x), i = 1,2.$$

$$\mu_{B_j}(y), j = 1,2. \quad (21)$$

Where, $\mu_{A_i} \mu_{B_j}$ are the MSF outputs obtained from the 1st layer.

The mathematical representation of Triangular MSF is given by Eq.22

$$\mu_{A_i}(x) = \max(\min(\frac{x - a_i}{b_i - a_i}, \frac{c_i - x}{c_i - b_i}), 0) \quad (22)$$

The Negative-Big (NEB), Negative medium (NEM), Zero (ZOE), Positive small (PES), Positive Big (PEB), Positive medium (PEM) and Negative-Small (NES) are considered as input. The inputs of MF are shown in Fig 6. Table 3 exhibits the fuzzy-rule-base.

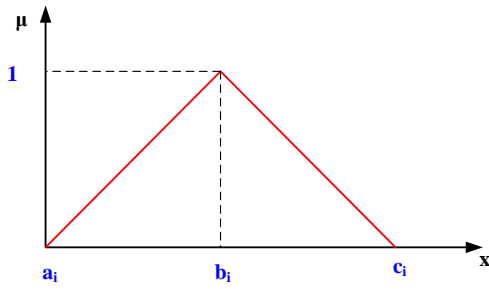
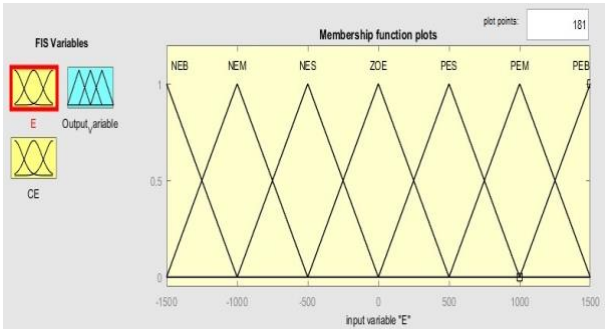
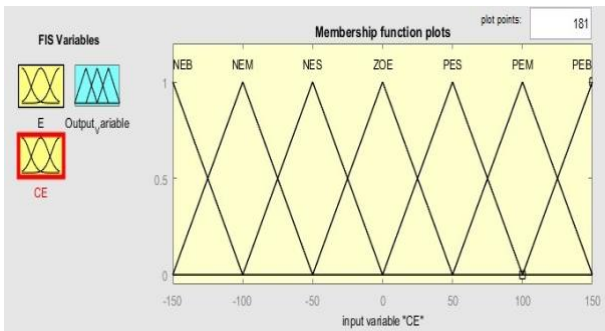


Fig.7. Traingular MSF



(a) MF for E



(b) MF for CE

Fig.8. Fuzzy MFS for E, CE

Table 5: Fuzzy Rule-base

E	CE						
	PEB	PEM	PES	ZOE	NES	NEM	NEB
NEB	ZOE	NES	NEM	NEB	NEB	NEB	NEB
NEM	PES	ZOE	NES	NEM	NEB	NEB	NEB
NES	PEM	PES	ZOE	NES	NEM	NEB	NEB
ZOE	PEB	PEM	PES	ZOE	NES	NM	NEB
PES	PEB	PEB	PEM	PES	ZOE	NES	NEM
PEM	PEB	PEB	PEB	PEM	PES	ZOE	NES
PEB	PEB	PEB	PEB	PEB	PEM	PES	ZOE

However, in the 2nd layer (weighting of fuzzy rules) the AND operator is applied and calculates the firing strength w_i by adopting MSF computed in 1st layer, whose output is calculated by Eq. (23).

$$w_k = \mu_{A_i}(x) * \mu_{B_j}(y), j = 1,2. \quad (23)$$

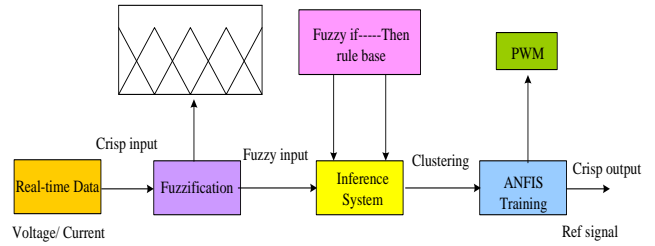


Fig.9. Overview of ANFIS

The normalization of values occurs in the 3rd layer received from the previous layer. Each node reaches normalization by evaluating the ratio of the k^{th} rule’s firing strength (truth values) to the summation of all rule’s firing strength is given Eq. (24).

$$\bar{w}_k = \frac{w_k}{w_1 + w_2} \quad k = 1,2. \quad (24)$$

The self-adaptive ability of the ANNC is carried out by applying the inference parameters (p_k, q_k, r_k) in the 4th layer (defuzzification) output is given by Eq. (25).

$$\bar{w}_i f_i = \bar{w}_i (p_k u + q_k v + r_k) \quad (25)$$

Lastly, at the 5th layer, inputs are get added up to produce the desired total ANFIS output by Eq. (26).

$$f = \sum_i \bar{w}_i f_i \quad (26)$$

Fig 8 shows the block diagram of the proposed ANFIS.

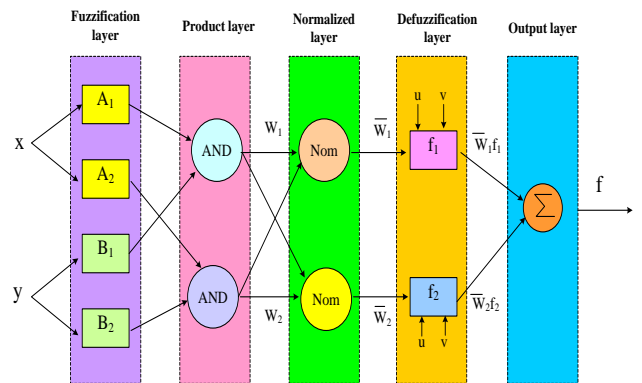


Fig. 10. Structure of ANFIS

The ANFIS is trained to maintain constant DLCV and to generate reference current signals. However, for keeping the DLCV constant, reference DLCV (V_{dc}^{ref}) is compared with the actual DLCV (V_{dc}); its error is chosen as input data, Δi_{dc} . Next, the load currents, like ($i_{l_{abc}}$) and DC loss component (Δi_{dc}), are considered as input while the reference currents ($i^{ref}_{sh_{abc}}$) are considered as target data as shown in Figure 11, and the structure with neurons selected are shown in Fig 12.

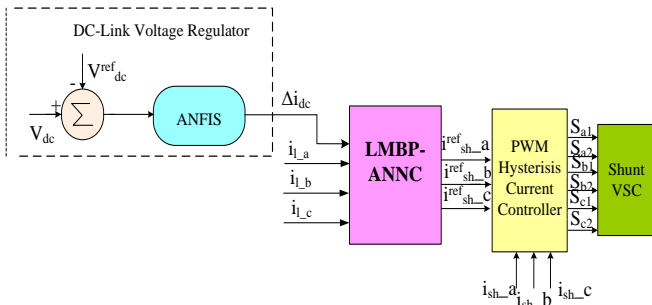


Fig. 11. Shunt VSC Controller

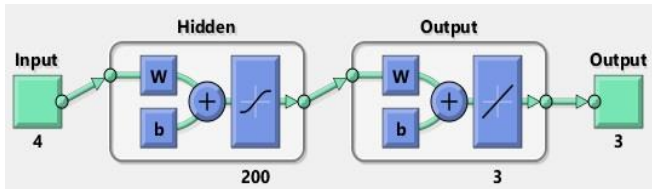


Fig. 12. ANNC for reference current generation.

3.2 Series VSC

The prominent role of SAPF is to suppress the grid side voltage distortions by injecting the suitable compensating voltage to maintain load voltage constant. Figure 11 exhibits the suggested series VSC reference signal generation scheme and Figure 12 shows the structure of ANN with a HIL of 200 neurons. To generate the reference voltage signals (V_{se}^{ref}) the supply voltages (V_{s_abc}) are considered as input data, while reference voltage is deemed into target data to ANN. The gating pulses for series VSC are generated with PWM.

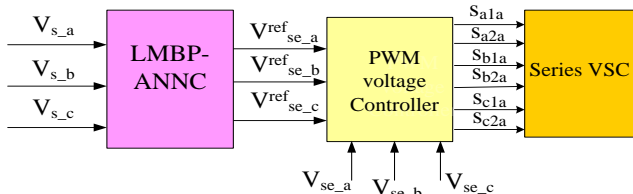


Fig. 13. Series-VSC controller

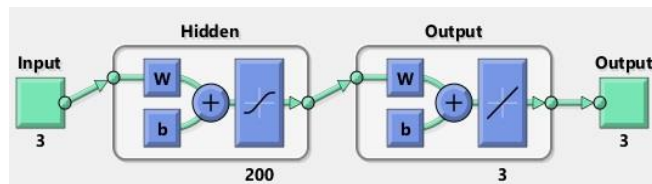


Fig. 14. Structure of ANNC for reference voltage generation.

4 Simulation and Results

The Simulink model of the proposed H-Bridge cascade 5L-UPQC with ANNC method is given in Fig 15. The selected system and the UPQC device parameters chosen are displayed in Table 6. However, four test cases with various permutations of voltage issues like sag, disturbance, swell, balanced and unbalanced loads with constant irradiation (G) and temperature of 25⁰c were selected to revel the working of developed ANNC on 5L-UPQC is given in Table 7. The

voltage sag, voltage swell, and voltage disturbance issues are considered for both case-1 and 2 and unbalanced grid supply issue is considered for case 3 and 4. However, in this work the reduction of current THD is regarded as objective which is obtained by developed ANN for reference signal generation, and optimal selection of shunt and series controller parameters for H-bridge cascade 5L-UPQC. The comparative analysis is carried out with PIC and SMC methods at DLCV balancing. The THD is evaluated by Eq. (27).

$$THD = \frac{\sqrt{(I_2^2 + I_3^2 + \dots + I_n^2)}}{I_1} \quad (27)$$

Where,

I_n = individual harmonic current distortion values in amps

I_1 = individual harmonic current distortion values in amps

I_2 = 2nd harmonic current distortion values in amps

The voltage sag/ swell ($V_{sag/swell}$) is evaluated by Eq. (28)

$$V_{sag/swell} = \frac{V_l - V_s}{V_l} = \frac{V_{se}}{V_l} \quad (28)$$

The injected voltage by series filter is calculated by Eq. (29)

$$V_{se} = V_l - V_s \quad (29)$$

The injected current by shunt filter is calculated by Eq. (30)

$$i_{sh} = i_i - i_s \quad (30)$$

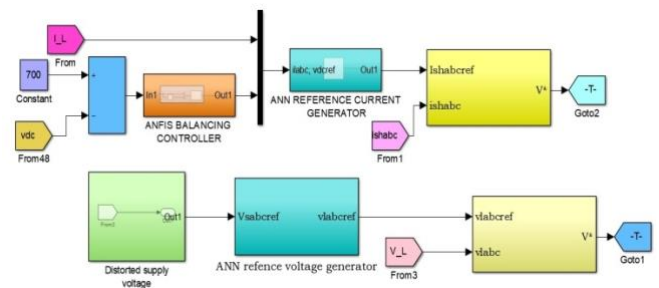


Fig. 15. Simulink model of the proposed ANN with ANFIS controller

Table 6: System and 5L-UPQC parameters

Grid Supply	V_s : 415Volts ;f: 50Hertz; R_s : 0.1ohm ; L_s : 0.15 mH
DC link capacitor & coupling inductors	C_{dc} :2200 μ F; L_{se} = 6 mH, L_{sh} =15mH
Loads	1. Balanced3 Φ nonlinear load: P_L =3kW, Q_L =0.5 kVAR 2. Un-balanced load: P_{La} =3kW, Q_{La} =9 kVAR; P_{Lb} =4kW, Q_{Lb} =10 kVAR; P_{Lc} =4kW, Q_{Lc} =10 Kvar

3. Rectifier bridged balanced RL Load: 30ohm & 20mH
4. Unbalanced rectifier RL Load: R_a, R_b, R_c : 10, 20 & 15 ohm; L_a, L_b, L_c : 9.50, 10.52, 18.50 mH

In case1, 30% of unbalanced sag/ swell and a disturbance are created in balanced supply voltage for 0.2 to 0.3 sec, 0.35 to 0.45sec, and 0.5 to 0.6 sec, respectively as shown in Fig 16(a). The developed ANN technique effectively notices the voltage dip, voltage raise, and disturbance, supplies the required compensating voltage through the interfacing transformer and maintains the load voltage constant. Besides, to exhibit the behavior of the shunt filter with ANNC, Loads 1 and 2 were considered. The load current waveform is unbalanced and non-sinusoidal, as seen in Fig 16(b). The developed method suppresses the distortions in the supply current, reducing the THD of source current to 2.26% and load voltage to 2.06%, much less than other techniques. In addition, it regulates DLCV stable as shown in Fig 16(c) for constant 1000W/ m² irradiation and 25⁰c of constant temperature.

In case 2, similar to case 1, the disturbance is introduced to the 30% of balanced sag and swell. However, the proposed system identifies it successfully and eliminates it by injecting the required compensating voltage, as demonstrated in in Figure 17(a). The load current signal was nonsinusoidal but balanced as shown in Figure 17(b), due to load 3. However, the proposed method reduces the THD of the source current to 2.12% and load voltage to 1.56%, which is lesser than other techniques. However, the suggested method maintains constant DLCV during load as well as irradiation variation, as Figure 17(c) shows.

Table 7: Test Cases studies considered for different loads

Condition	Case1	Case2	Case3	Case4
Balanced V_s	✓	✓		
Balanced V_{Sag} , V_{Swell} , disturbance		✓		

Unbalanced V_{Sag} , V_{Swell} , disturbance	✓			
Unbalanced V_s			✓	✓
Current	✓	✓	✓	✓
Constant Irradiation 1000W/m ² and 25 ⁰ c temperature	✓		✓	
Variable irradiation and 25 ⁰ c Temperature		✓		✓
DLCV	✓	✓	✓	✓
THD (both V and I)	✓	✓	✓	✓
Load1	✓			
Load 2	✓			
Load 3		✓	✓	
Load 4			✓	✓

In case3, unbalanced grid voltage has been supplied with load 3 and 4 acting simultaneously. It is clearly exhibited from the Fig. 18 that proposed system handles imbalances effectively and provides constant balanced voltage to load. Due to the selected load the load currents were observed to be sinusoidal and imbalance in phases. The current THD was reduced to 3.72% and voltage to 3.01%. However, the suggested method maintains constant DLCV.

In case 4, the unbalanced grid voltage is selected with load 4, the developed systems eliminates imperfections in supply voltage and improves the THD to 1.59% in addition to maintain DLCV stable during load and irradiation variation as shown in Fig. 19. The THD spectrum of case1 phase a is exhibited in Fig 20.

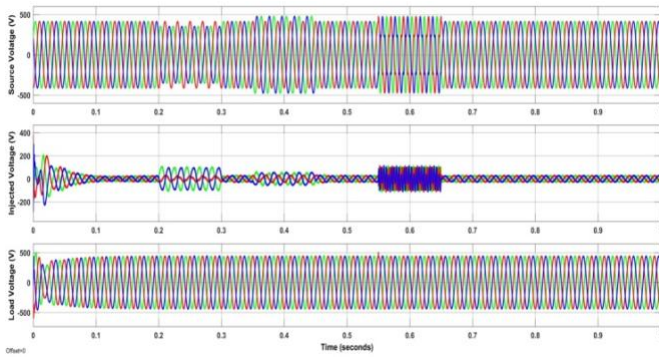
Table 8: THD comparison

Method [Ref]	THD						
	Source Current			Load Voltage			
	Phase-a	Phase-b	Phase-c	Phase-a	Phase-b	Phase-c	
Proposed Scheme with ANFIS controller	2.26	2.49	2.31	2.06	2.11	2.24	
Case-1 Proposed Scheme with PIC	3.42	3.12	3.01	2.14	2.75	2.97	
Proposed Scheme with SMC	3.07	2.89	2.99	2.41	2.87	2.99	
3L-UPQC with proposed scheme	3.12	3.41	3.25	2.18	2.51	2.46	
2L-UPQC with proposed scheme	3.58	3.81	3.42	2.98	2.84	2.73	

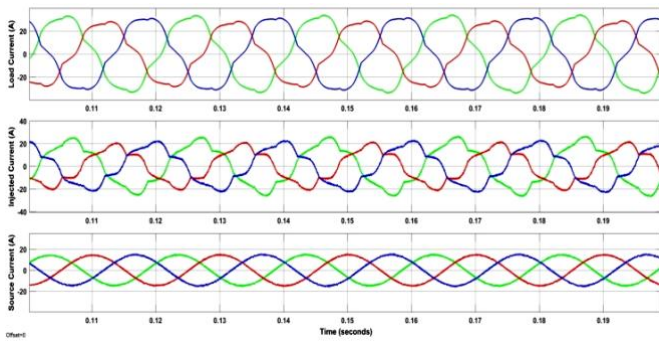
	3L-UPQC with SRF theory	3.52	3.87	3.74	3.14	3.07	2.94
	2L-UPQC with p-q theory	3.64	3.91	3.89	3.28	3.13	2.14
	2L-UPQC [29]	5.42	5.43	5.61	4.03	3.86	4.04
	3L-UPQC [29]	4.72	4.45	4.86	3.37	3.27	3.36
	5L-UPQC [29]	3.85	4.09	4.40	3.02	2.97	3.03
	2L-UPQC-SRF [29]	5.47	6.07	5.95	4.45	4.76	4.99
	3L-UPQC-SRF [29]	5.55	6.06	4.94	4.22	4.24	4.43
	5L-UPQC-SRF [29]	4.55	5.45	4.32	3.83	3.98	4.22
	ANN [7]	3.72	--	--	--	--	--
	Proposed method	2.12	2.33	2.39	1.56	1.67	1.43
	(ANN with ANFIS)						
	Proposed Scheme with PIC	2.36	2.57	2.90	2.01	2.31	1.61
	Proposed Scheme with SMC	2.29	2.57	2.74	1.91	1.77	1.84
Case-2	3L-UPQC with proposed scheme	2.93	2.75	2.64	2.91	2.84	2.73
	2L-UPQC with proposed scheme	3.17	3.05	3.54	3.41	3.22	3.11
	3L-UPQC with SRF theory	3.58	3.12	3.54	3.16	3.35	3.47
	2L-UPQC with p-q theory	4.03	4.26	4.51	4.34	4.12	4.48
	ANN [7] case4	4.55	--	--	--	--	--
	Proposed method	3.73	3.72	4.14	3.01	3.12	3.41
Case-3	(ANN with ANFIS)						
	Proposed Scheme with PIC	3.97	3.88	3.99	3.14	4.01	3.64
	Proposed Scheme with SMC	3.08	3.77	4.18	3.04	3.98	4.05
	3L-UPQC with proposed scheme	3.97	3.69	4.17	3.01	3.45	3.67
	2L-UPQC with proposed scheme	4.36	4.21	4.05	3.36	3.71	3.76
	3L-UPQC with SRF theory	4.71	4.62	4.93	3.87	3.68	3.94
	2L-UPQC with p-q theory	4.83	4.78	4.99	4.32	4.57	4.35
	Proposed method	1.59	1.21	1.60	2.85	2.47	2.65
Case-4	(ANN with ANFIS)						
	Proposed Scheme with PIC	1.77	1.87	2.96	3.41	3.99	3.87
	Proposed Scheme with SMC	1.61	1.79	2.65	3.01	4.01	3.04
	3L-UPQC with proposed scheme	2.97	2.36	2.36	2.91	2.85	2.77
	2L-UPQC with proposed scheme	3.12	3.58	3.61	3.54	3.67	3.43
	3L-UPQC with SRF theory	4.71	3.67	3.31	3.65	3.68	3.44

2L-UPQC with p-q theory	4.67	4.97	4.57	4.78	4.27	4.69
-------------------------	------	------	------	------	------	------

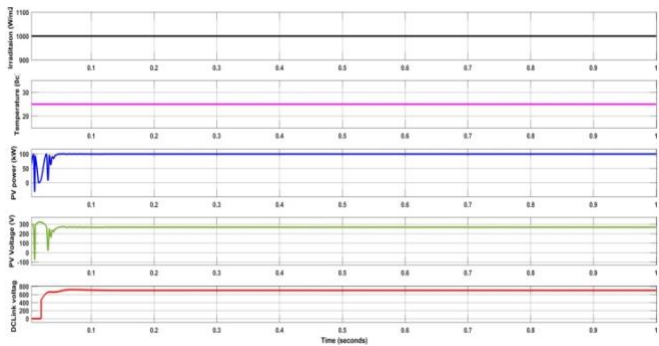
*Proposed scheme = ANN based reference signal generation



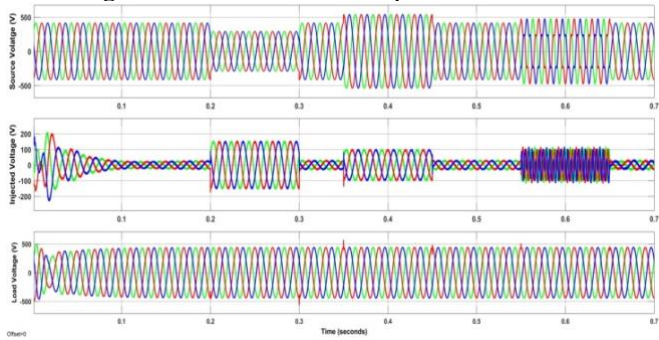
(a) V_S, V_{se}, V_l



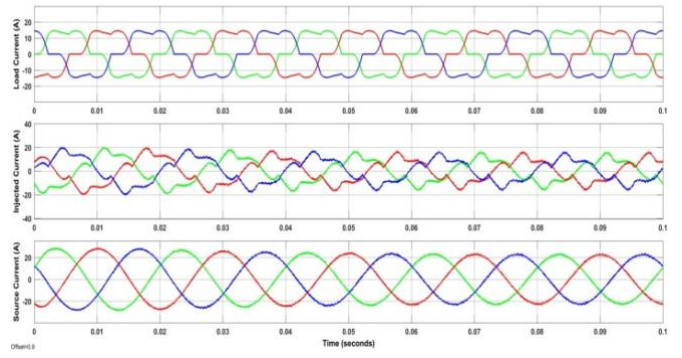
(b) i_l, i_{sh}, i_S



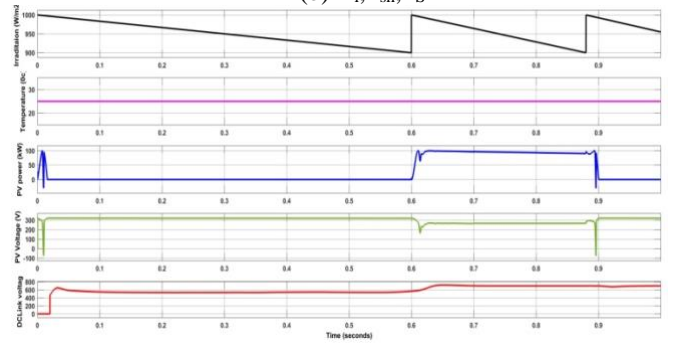
(C) G, T, P_{PV}, V_{PV}, DLCV
Fig.16. Waveforms of developed method for case-1



(a) V_S, V_{se}, V_l

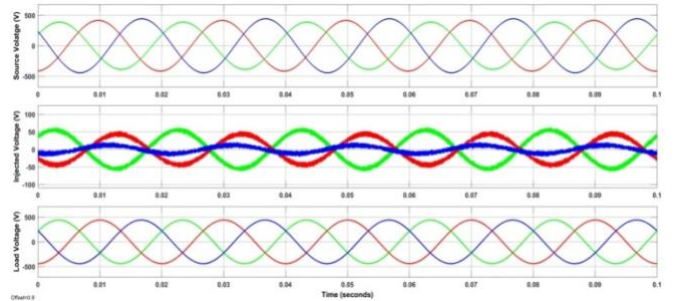


(b) i_l, i_{sh}, i_S

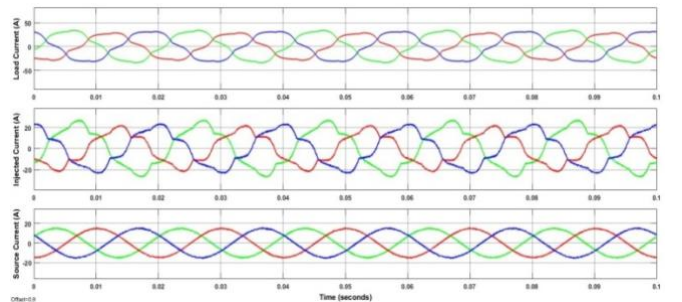


(c) G, T, P_{PV}, V_{PV}, DLCV

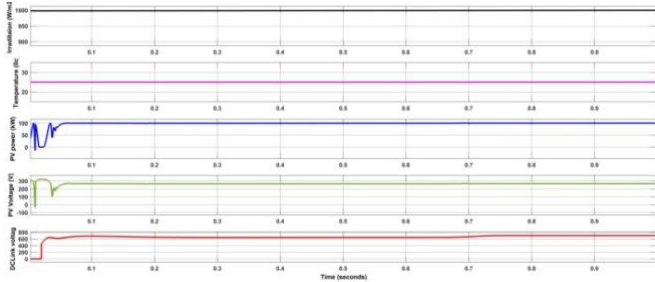
Fig.17. Waveforms of developed method for case-2



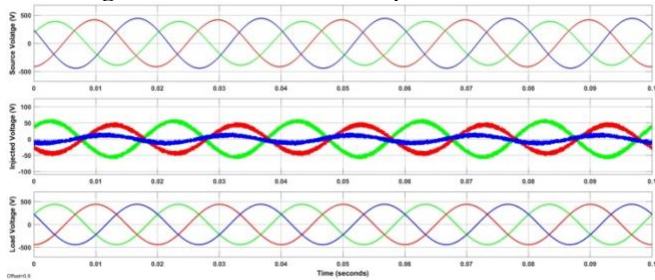
(a) V_S, V_{se}, V_l



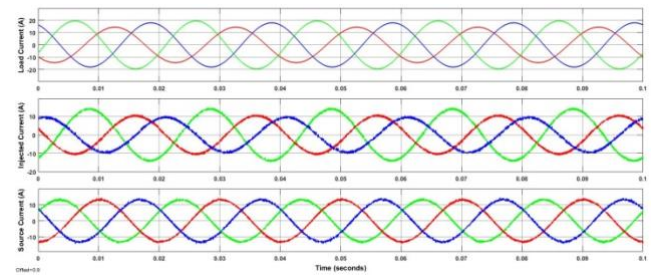
(b) i_l, i_{sh}, i_S



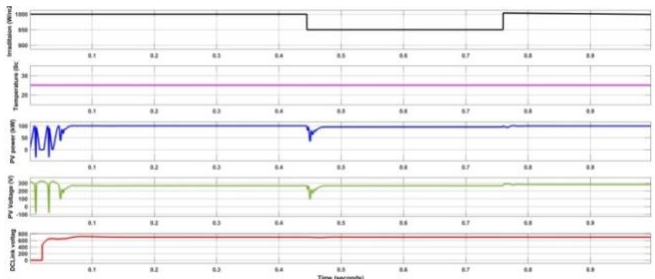
(c) $G, T, P_{PV}, V_{PV}, DLCV$
Fig.18. Waveforms of developed method for case-3



(a) V_S, V_{se}, V_l



(b) i_l, i_{sh}, i_S



(a) $G, T, P_{PV}, V_{PV}, DLCV$
Fig.19. Waveforms of developed method for case-4

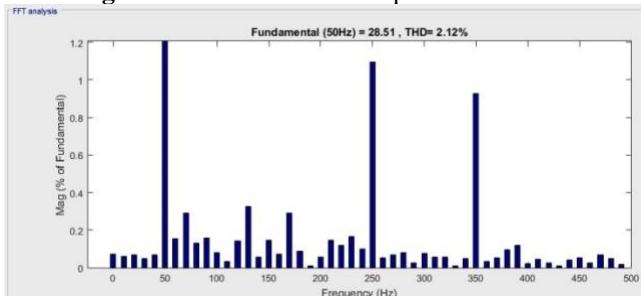


Figure 20: Current THD spectrum for case2 phase-a

5 Conclusion

This paper proposes an ANNC-based new method for a solar battery connected to UPQC. The LMBP-trained ANN controller is presented to produce the required reference

signals for shunt series VSC’s to avoid the traditional abc-dq0- $\alpha\beta$ conversions. In addition, the ANFIS hybrid controller is adapted for DLCV balancing. However, the developed H bridge cascade 5L-UPQC maintains constant DLCV during loads variations, suppresses the source current and load voltage harmonics and improves the current and voltage waveform’s shape, and eliminates the fluctuations of supply voltage (disturbance, sag and swell). The comparison is carried out with ANN, PIC and SMC controllers for DLCV balancing and other methods available in the literature. The results of the two test cases show that the developed method provides much lower THD than other methods in literature and within acceptable levels. The developed method can be carried out using metaheuristic optimization control scheme in the future in addition to the microgrid.

References

1. D. Yang , Z. Ma , X. Gao , Z. Ma, E. Cui, “Control Strategy of Intergrated Photovoltaic-UPQC System for DC-Bus Voltage Stability and Voltage Sags Compensation”, *Energies*, Vol. 12, No. 20, pp. 4009, Oct-2019.
2. G Arunsankar, and S. Srinath, “Optimal controller for mitigation of harmonics in hybrid shunt active power filter connected distribution system: An EGOANN technique”, *Journal of Renewable and Sustainable Energy*, Vol. 11, No. 2, pp. 025507, April-2019.
3. A. Mishra , S. R. Das , P. K. Ray , R. K. Mallick, A. Dillip ,K. Mishra, “PSO-GWO Optimized Fractional Order PID Based Hybrid Shunt Active Power Filter for Power Quality Improvements”, *IEEE Access*, Vol.8, pp. 74497 - 74512, May-2020
4. D. Mahdi and G. Gorel, “Design and Control of Three-Phase Power System with Wind Power Using Unified Power Quality Conditioner”, *Energies* 2022, Vol. 15, No. 19, pp. 7074, Sep-2022.
5. X. Zhao ,X. Chai, X. Guo, A. Waseem, X. Wang and C. Zhang, “Impedance Matching-Based Power Flow Analysis for UPQC in Three-Phase Four-Wire Systems”, *Energies*, Vol.14, No. 9, pp. 2702, May-2021
6. Y. Hoon, M. A. MohdRadzi, M. Hassan, N.F. Mailah, “Control Algorithms of Shunt Active Power Filter for Harmonics Mitigation: A Review”, *Energies*, Vol.10, No.12, PP. 2038, Dec-2017.
7. K. Srilakshmi, K. K. Jyothi, G. Kalyani & Y. S.P Goud. “Design of UPQC with Solar PV and Battery Storage Systems for Power Quality Improvement. *Cybernetics and Systems: An International Journal*”, March-2023.
8. T. Chiao Lin, B. Simachew, “Intelligent Tuned Hybrid Power Filter with Fuzzy-PI Control”, *Energies*, Vol. 15, No. 12, pp. 4371, June-2022.
9. O.E Okwakol , Z. Hui Lin 1, M. Xin, K. Premkumar, Alukaka, “Neural Network Controlled Solar PV Battery Powered Unified Power Quality Conditioner for Grid Connected Operation”, *Energies*, Vol. 15, No. 18, PP. 6825, Sep-2022.
10. K. Srilakshmi, A Pandian and A. Palanivelu, “Fuzzy Based Hybrid Controller for UPQC with Wind and Battery Storage Systems, *International Journal of Electronics*”, Aug- 2023.

11. K. Chandrasekaran, J. Selvaraj, C. Amaladoss, L. Veerapan, "Hybrid renewable energy based smart grid system for reactive power management and voltage profile enhancement using artificial neural network, *Energy Sources, Part A: Recovery, Utilization, and Environmental Effects*", Vol. 43, No. 19, pp. 2419–2442, sep-2022.
12. B. Aljafari, K. Rameshkumar, V. Indragandhi, S. Rama chandran, "A Novel Single-Phase Shunt Active Power Filter with a Cost Function Based Model Predictive Current Control Technique", *Energies*, Vol.15, No. 13, pp. 4531, Jun-2022.
13. K. Sarker, D. Chatterjee & S. K. Goswami, "A modified PV-wind-PEMFCS-based hybrid UPQC system with combined DVR/STATCOM operation by harmonic compensation", *International Journal of Modeling and Simulation*, Vol.41, No.4, pp. 243-255, March 2020.
14. Y. Hoon, M. A. Mohd Radzi, M. A. A. Mohd Zainuri, M. Zawawi, "Shunt Active Power Filter: A Review on Phase Synchronization Control Techniques", *Electronics*, Vol. 8, No. 7, pp. 791, July-2019.
15. A. Szromba, "The Unified Power Quality Conditioner Control Method Based on the Equivalent Conductance Signals of the Compensated Load", *Energies*, Vol. 13, No. 23, pp. 6298, Nov-2020.
16. A. Nafeh, A. Heikal, R. A. El-Sehiemy, W. A.A. Salem, "Intelligent fuzzy-based controllers for voltage stability enhancement of AC-DC micro-grid with D-STATCOM", *Alexandria journal of Engineering*, Vol.61, No. 3, pp. 2260-2293, March-2022.
17. M. Nicola, C. Nicola, D. Sacerdoțianu and A. Vintilă, "Comparative Performance of UPQC Control System Based on PI-GWO Fractional Order Controllers, and Reinforcement Learning Agent", *Electronics*, Vol. 12, No. 3, pp. 494, Jan-2023.
18. A. A. Imam, R. Sreerama Kumar, Yusuf A. Al-Turk, "Modeling and Simulation of a PI Controlled Shunt Active Power Filter for Power Quality Enhancement Based on P-Q Theory", *Electronics*, Vol. 9, No. 4, pp. 637, April-2020.
19. Sayed J.A, R. A, Sabha, K. J. Ranjan, "Biogeography based optimization strategy for UPQC PI tuning on full order adaptive observer based control. *IET Generation, Transmission & Distribution*, Vol. 15, No.2 pp. 279-293, Jan-2021.
20. U.K. Renduchintala, C. Pang, K.M. Tatikonda, L. Yang, "ANFIS-Fuzzy logic based UPQC in interconnected microgrid distribution systems: modeling, simulation and implementation", *The Journal of Eng*, Vol. 2021, No. 1, pp. 6–18, Feb-2021.
21. Rajesh, P, Shajin, F.H, Umasankar. L, "A Novel Control Scheme for PV/WT/FC/Battery to Power Quality Enhancement in Micro Grid System: A Hybrid Technique", *Energy Sources, Part A: Recovery, Utilization, and Environmental Effects* 2021, pp. 1-18.
22. C. Pazhanimuthu, S. Ramesh, "Grid integration of renewable energy sources (RES) for power quality improvement using adaptive fuzzy logic controller based series hybrid active power filter (SHAPF)", *Journal of Intelligent & Fuzzy Systems*, Vol. 35, No.1, pp. 749–766, July-2018.
23. S. Mahaboob, S. Kumar Ajithan, S. Jayaraman, "Optimal design of shunt active power filter for power quality enhancement using predator-prey based firefly optimization", *Swarm and Evolutionary computation*, Vol. 44, 522-533, (2019).
24. K. Srilakshmi, C. Narahari Sujatha, P. Balachandran, L. Mihet-Popa, and N. Udaya Kumar, "Optimal Design of an Artificial Intelligence Controller for Solar-Battery Integrated UPQC in Three Phase Distribution Networks", *Sustainability*, Vol. 14, No. 21, Oct-2022.
25. A. Sakthivel, P. Vijayakumar, A. Senthilkumar, L. Lakshminarasimman, S. Paramasivam, "Experimental investigations on ant colony optimized pi control algorithm for shunt active power filter to improve power quality", *Control Engineering Practice*. Vol.42, pp. 153-169, Dec-2015.
26. H. Kenjrawy, C. Makdisie, I. Houssamo, N Mohammed, "New Modulation Technique in Smart Grid Interfaced Multilevel UPQC-PV Controlled via Fuzzy Logic Controller", *Electronics*, Vol.11, No.6, pp. 919, March-2022.
27. K. Srilakshmi, N. Srinivas, B. Praveen, J. Ganesh Prasad Reddy, S. Gaddameedhi, N. Valluri, S. Selvarajan, "Design of Soccer League Optimization Based Hybrid Controller for Solar-Battery Integrated UPQC", *IEEE Access*, Vol. 10, pp. 107116-107136, Oct-2022.
28. S. Koganti, K.K. Jyothi and S. Salkuti, "Design of Multi-Objective-Based Artificial Intelligence Controller for Wind/Battery-Connected Shunt Active Power Filter, *Algorithms*, Vol. 15, No. 8, pp. 256, 2022, July-2022.
29. S. Vinnakoti, V. Reddy Kota, "Implementation of artificial neural network based controller for a five-level converter based UPQC", *Alexandria Engineering Journal*, Elsevier, Vol .57, No. 3, pp.1475-1488, March-2017.
30. A. Ramadevi, K. Srilakshmi, P. Balachandran, Ilhami Colak, C. Dhanamjayulu, and Baseem Khan, "Optimal Design and Performance Investigation of Artificial Neural Network Controller for Solar- and Battery-Connected Unified Power Quality Conditioner", *International Journal of Energy Research*, Vol. 2023, PP. 3355124, April-2023.
31. M. A. Mansoor, K. Hasan, M.M. Othman, S. Z. B. M. Noor, and I. Musirin. "Construction and performance investigation of three phase solar PV and battery energy storage system integrated UPQC", *IEEE Accesses*, Vol.8, pp. 103511 – 103538,
32. Z. Ming, W. Ru, W. Qiang, Cui Jian, "Control Method for Power Quality Compensation Based on Levenberg-Marquardt Optimized BP Neural Networks", 2006 CES/IEEE 5th International Power Electronics and Motion Control Conference.
33. F. Ayadi; I. Colak; I. Garip, H. Bulbul, "Impacts of Renewable Energy Resources in Smart Grid", 8th International Conference on Smart Grid, Paris, pp. 183-188, June 2020.
34. I. Colak; R. Bayindir, S. Sagioglu, "The Effects of the Smart Grid System on the National Grids", 8th International Conference on Smart Grid, Paris, pp. 122-126, June 2020.
35. S. Jaber, A. M. Shakir, "Design and Simulation of a Boost-Microinverter for Optimized Photovoltaic System Performance", *International Journal of Smart Grid*, Vol. 5, No. 2, pp. 1-9, June 2021.

36. S. S. Dash, "Tutorial 1: Opportunities and challenges of integrating renewable energy sources in smart" 6th International Conference on Renewable Energy Research and Applications, San Diego, CA, USA, 5-8 Nov. 2017.
37. M. Tsai, C. Chu, W. Chen, "Implementation of a Serial AC/DC Converter with Modular Control Technology", 7th International Conference on Renewable Energy Research and Applications, Paris, France, pp. 245-250, Oct. 2018.
38. A. Belkaid, I. Colak, K. Kayisli, R. Bayindir, Improving PV System Performance Using High Efficiency Fuzzy Logic Control, 8th International Conference on Smart Grid, Paris, pp.152-156, June 2020.
- 39.